RSC Advances

ROYAL SOCIETY OF CHEMISTRY

www.rsc.org/advances

RSC Advances

Dynamic Article Links ►

Cite this: DOI: 10.1039/c0xx00000x

www.rsc.org/xxxxxx

PAPER

Poly(γ-glutamic acid)-stabilized iron oxide nanoparticles: Synthesis, characterization and applications for MR imaging of tumors†

Zhibo Yu,[a,1] Chen Peng,[b,1] Yu Luo,[c] Jianzhi Zhu,[c] Chen Chen,[c] Mingwu Shen,[c] Xiangyang Shi[a,c,*]

Received (in XXX, XXX) Xth XXXXXXXXX 20XX, Accepted Xth XXXXXXXXX 20XX
DOI: 10.1039/b000000x

We report a facile poly(γ-glutamic acid) (PGA)-assisted "one-step" synthesis of Fe_3O_4 nanoparticles (NPs) for *in vivo* magnetic resonance (MR) imaging of tumors. In this work, a mild reduction method was employed to synthesize Fe_3O_4 NPs in the presence of PGA. We show that the formed PGA-stabilized Fe_3O_4 NPs (Fe_3O_4-PGA NPs) display good water-dispersibility, colloidal stability, relatively high r_2 relaxivity (333.7 $mM^{-1}s^{-1}$), and good cytocompatibility and hemocompatibility in the studied concentration range. Cellular uptake results demonstrate that the Fe_3O_4-PGA NPs have minimum macrophage cellular uptake, which is beneficial for them to escape the uptake by the reticuloendothelial system *in vivo*. Importantly, the formed Fe_3O_4-PGA NPs can be used as a contrast agent for MR imaging of tumors *in vivo* thanks to the passive enhanced permeability and retention effect. The developed Fe_3O_4-PGA NPs may hold great promise to be used as a contrast agent for MR imaging of different biological systems.

Introduction

Magnetic resonance (MR) imaging has been widely applied in clinical diagnosis due to its high spatial resolution and tomographic capabilities.[1] For improved MR imaging applications, contrast agents have been usually required.[2-4] Superparamagnetic iron oxide (Fe_3O_4) nanoparticles (NPs) have been employed as T_2-weighted MR contrast agents due to their capacity to shorten the T_2 relaxation time of water protons.[5-7] In general, the developed Fe_3O_4 NPs should have excellent colloidal stability, biocompatibility, and the ability to escape the nonspecific uptake by reticuloendothelial system (RES). An effective approach to meet the above requirements is to modify the surface of the Fe_3O_4 NPs with hydrophilic polymers.[8, 9] The commonly employed polymers such as dextran,[9-11] dendrimers,[1, 4, 12-14] chitosan,[15, 16] polyethylene glycol (PEG),[17, 18] polyethyleneimine (PEI)[19-21] have offered meaningful improvements. However, most of the employed approaches are quite time-consuming or involve in multiple-step processes, and some of the approaches even require high temperature or high pressure conditions. Development of new polymer-coated Fe_3O_4 NPs with a simple one-step method for MR imaging applications still remains a great challenge.

Poly(γ-glutamic acid) (PGA) produced by several Bacillus species is a biodegradable and biocompatible polymer with good water-retention ability due to the presence of a large number of carboxyl groups on its side chain.[22, 23] PGA have been widely applied in different biomedical fields such as drug delivery,[22, 24-26] wound dressing,[27] and tissue engineering.[28-30] Nevertheless, there have been no studies concerning the use of PGA as a stabilizing agent to form Fe_3O_4 NPs for biomedical applications.

In our previous work, we have shown that PEI-coated Fe_3O_4 NPs can be prepared *via* a facile hydrothermal approach[31] and the PEI-coated Fe_3O_4 NPs can be further functionalized with different biomolecules for MR imaging applications.[8, 9, 32] Recently, Hong *et al.*[33] reported a mild reduction method to prepare superparamagnetic Fe_3O_4 NPs that displayed a superhigh r_2 relaxivity. Based on this work, we have developed a mild one-step method to prepare PEI-coated Fe_3O_4 NPs that can be further modified with targeting ligands for targeted MR imaging of tumors.[34, 35] These prior successes prompt us to hypothesize that PGA-coated Fe_3O_4 NPs may also be prepared using the above mild reduction method for MR imaging applications.

In this present study, we developed a facile one-step method to produce PGA-stabilized Fe_3O_4 NPs for MR imaging of tumors. In the presence of PGA, mild reduction of Fe(III) salt using Na_2SO_3 as a reducing agent resulted in the formation of PGA-stabilized Fe_3O_4 NPs (Fe_3O_4-PGA NPs). The formed Fe_3O_4-PGA NPs were well characterized *via* different methods. The *in vitro* hemocompatibility, cytocompatibility, and macrophage cellular uptake of the particles were then thoroughly investigated. Finally the potential to use the Fe_3O_4-PGA NPs as a contrast agent for MR imaging of a xenografted tumor model was assessed. To our knowledge, this is the first report related to the mild-reduction synthesis of Fe_3O_4-PGA NPs for MR imaging applications.

Experimental

Materials

PGA (M_w = 1000 kDa) was purchased from Nanjing Saitesi Co., Ltd. (Nanjing, China). Ferric chloride hexahydrate ($FeCl_3 \cdot 6H_2O$ > 99%), ammonia (25-28% NH_3 in water solution) and all the other chemicals and solvents were obtained from Sinopharm Chemical Reagent Co., Ltd. (Shanghai, China). 3-(4,5-Dimethylthiazol-2-yl)-2,5-diphenyltetrazolium bromide (MTT) was acquired from Shanghai Sangon Biological Engineering Technology & Services Co., Ltd. (Shanghai, China). All chemicals were used as received. HeLa cells (a human cervical cancer cell line) were obtained from Institute of Biochemistry and Cell Biology, the Chinese Academy of Sciences (Shanghai, China). Dulbecco's Modified Eagle Medium (DMEM), fetal bovine serum (FBS), penicillin, and streptomycin were purchased from Hangzhou Jinuo Biomedical Technology (Hangzhou, China). Water used in all experiments was purified by a Milli-Q Plus 185 water purification system (Millipore, Bedford, MA) with a resistivity higher than 18.2 MΩ.cm. Regenerated cellulose dialysis membranes (molecular weight cut-off, MWCO = 8 000~14 000) were obtained from Shanghai Yuanye Biotechnology Corporation (Shanghai, China).

Synthesis of the Fe_3O_4-PGA NPs

The Fe_3O_4-PGA NPs were synthesized according to the procedures reported in the literature with slight modification.[33] Briefly, $FeCl_3 \cdot 6H_2O$ (1.2 g) dissolved in water (20 mL) was placed in a 500-mL three-necked flask. Under vigorous stirring, nitrogen gas was bubbled for 5 min. Then PGA (180 mg) dissolved in water (40 mL) was added into the flask under stirring for 5 min, followed by dropwise addition of an aqueous solution of Na_2SO_3 (200 mg, 10 mL). When the solution color changed to yellow, the reaction mixture was heated to 60 ^oC in a water bath, and ammonia (1 mL) was rapidly injected into the flask under vigorous stirring. After 30 min, the reaction mixture was cooled down to room temperature (25 ^oC). The product was centrifuged (8000 rpm for 5 min) and the black precipitate was dialyzed against water (3 times, 2 L) for 3 days using a dialysis membrane with an MWCO of 8000~14000. The obtained Fe_3O_4-PGA NPs dispersed in water were separated into 2 parts: One part was lyophilized for further characterization and the other part remained in water and stored at 4 ^oC before further biomedical uses. For comparison, naked Fe_3O_4 NPs without the stabilization by PGA were also synthesized according to the above procedures.

Characterization techniques

The crystalline structure of the Fe_3O_4-PGA NPs was characterized *via* X-ray diffraction (XRD). XRD was performed using a D/max 2550 PC X-ray diffractometer (Rigaku Cop., Tokyo, Japan) with Cu Kα radiation (λ = 0.154056 nm) at 40 kV and 200 mA and a 2θ scan range of 10-80°. The morphology of the Fe_3O_4-PGA NPs was characterized with transmission electron microscopy (TEM, JEOL 2010F, Tokyo, Japan) at an accelerating voltage of 200 KV. TEM samples were prepared by depositing a drop (5 μL) of particle suspension in water onto carbon-coated copper grid and air dried before measurements. The structure of the Fe_3O_4-PGA NPs was confirmed by Fourier transform infrared (FTIR) spectroscopy (Nicolet Nexus 670, Nicolet Thermo, Madison, WI). Dried samples were mixed with ground KBr crystals and pressed as pellets before measurements. Thermogravimetric analysis (TGA) was conducted using a TG 209 F1 (NETZSCH Instruments Co., Ltd, Selb/Bavaria, Germany) thermal gravimetric analyzer to quantify the composition of the particles. The sample was heated from room temperature to 900 ^oC under N_2 atmosphere at a heating rate of 10 ^oC min^{-1}. The Fe concentration of the Fe_3O_4-PGA NPs was analyzed by a Leeman Prodigy Inductively Coupled Plasmon-Optical Emission Spectroscopy (ICP-OES, Hudson, NH).[31] A Malvern Zetasizer Nano ZS model ZEN3600 (Worcestershire, UK) equipped with a standard 633 nm laser was used to measure the surface potential and hydrodynamic size of the particles. T_2 relaxomertry was performed using a 0.5-T NMI20-Analyst NMR Analyzing and Imaging system (Shanghai Niumag Corporation, Shanghai, China). The Fe concentration of the particles was set in a range of 0.004~0.064 mM. The instrument parameters were set as follows: point resolution = 156 mm × 156 mm; point section thickness = 1 mm; TR = 4500 ms; TE = 60 ms; and number of excitations = 1. The r_2 relaxivity was calculated by linear fitting of the inverse T_2 ($1/T_2$) relaxation time as a function of Fe concentration.

Hemolysis assay

Fresh human blood sample stabilized with EDTA was provided by Shanghai Tenth People's Hospital (Shanghai, China) and approved by the Ethical Committee of Shanghai Tenth People's Hospital. The hemolysis assay was performed according to protocols reported in the literature.[31, 36] Briefly, the fresh human blood sample was centrifuged and purified to obtain the suspension of human red blood cells (HRBCs) dispersed in normal saline (NS). The HRBC suspension (0.1 mL) was added to 0.9 mL water as a positive control, 0.9 mL NS as a negative control, and 0.9 mL NS containing the Fe_3O_4-PGA NPs with different Fe concentrations (50-450 μgmL^{-1}). The samples were gently shaken, then kept still for 2 h at room temperature. The photo of each sample was taken after centrifugation (10 000 rpm, 1 min), and the absorbance of the supernatants (hemoglobin) for each sample was collected by a Lambda 25 UV-vis spectrophotometer (PerkinElmer, Boston, MA). The hemolysis percentage of each sample was calculated by dividing the difference in absorbances at 541 nm between each sample and the negative control by the difference in absorbances at 541 nm between the positive and negative controls.

Cell culture

HeLa cells or Raw 264.7 cells were cultured and passaged in DMEM supplemented with 10% heat-inactivated FBS, penicillin (100 UmL^{-1}), and streptomycin (100 UmL^{-1}) at 37 ^oC and 5% CO_2.

Cytotoxicity assay

MTT assay was used to quantify the viability of HeLa cells treated with the naked Fe_3O_4 or Fe_3O_4-PGA NPs at different Fe concentrations according to the literature.[32] HeLa cells were seeded in a 96-well plate at a density of 1×10^4 cells per well with 200 μL DMEM. After overnight incubation, the medium was replaced with 200 μL fresh medium containing NS, Fe_3O_4 NPs, or Fe_3O_4-PGA NPs at different Fe concentrations. After 24 h incubation at 37 ^oC, MTT (20 μL) was added to each well and the assay was performed according to the manufacturer's instructions. For each sample, mean and standardard deviation of 5 parallel wells were reported.

To qualitatively assess the cytocompatibility of the Fe_3O_4-PGA NPs, the morphology of HeLa cells treated with the Fe_3O_4-PGA NPs at different Fe concentrations for 24 h was observed by phase contrast microscopy (Leica DM IL LED inverted phase contrast microscope).

Macrophage cellular uptake

Raw 264.7 cells were seeded in a 12-well plate at a density of 1×10^5 cells per well with 2 mL DMEM. After overnight incubation to bring the cells to confluence, the medium was replaced with 2 mL fresh medium containing NS, Fe_3O_4 NPs, or Fe_3O_4-PGA NPs at different Fe concentrations (10 or 100 μgmL^{-1}, 2 wells in parallel for each concentration). After 4 h incubation at 37 ^oC, the medium was removed and the cells were washed with NS for 3 times. Subsequently, the cells were trypsinsized, resuspended in DMEM, and counted by hemacytometry. The cells were then collected by centrifugation, lysed using an aqua regia solution (0.5 mL) for 2 h, and diluted with 2 mL water before quantification of the Fe concentration *via* ICP-OES.

***In vivo* MR imaging of a xenografted tumor model**

Male 4- to 6-week-old BALB/c nude mice (18-21 g) were provided by Shanghai Slac Laboratory Animal Center (Shanghai, China). All animal experiments were carried out according to protocols approved by the institutional committee for animal care, and also in accordance with the policy of the National Ministry of Health. The mice were subcutaneously injected with 2×10^6 HeLa cells/mouse in the left back. After approximately 3 weeks, when the tumor nodules reached a volume of 0.8-1.4 cm^3, the mice were anesthetized by intraperitoneal injection of pentobarbital sodium (40 $mgkg^{-1}$). Then the Fe_3O_4-PGA NPs (dispersed in 100 µL NS) were intravenously delivered into each tumor-bearing mouse *via* the tail vein (100 µg Fe per mouse). MR scanning was performed using a Siemens superconductor clinical MR system with a custom-built rodent receiver coil (Chenguang Med Tech, Shanghai, China) under the parameters of 2 mm slice thickness, 2000/81.9 ms TR/TE, and 6×6 cm FOV. Two-dimensional (2D) spin-echo T_2-weighted MR images were obtained before injection and at 2, 4, and 6 h postinjection, respectively. The MR imaging was quantitatively characterized by MR signal to noise ratio using the Siemens workstation. The MR intensity of air was identified to be the noise.

***In vivo* biodistribution**

The Fe_3O_4-PGA NPs (100 µL in NS) were intravenously delivered into each tumor-bearing mouse *via* the tail vein (100 µg Fe per mouse). At 2, 4, and 6 h postinjection, each mouse was anesthetized and the heart, liver, spleen, lung, kidney and tumor were extracted, weighed, and digested by aqua regia solution (nitric acid/hydrochloric acid, v/v = 1:3). Fe content in each organ was determined by ICP-OES. The mice injected with 100 µL NS were used as control.

Results and discussion

Synthesis and Characterization of the Fe_3O_4-PGA NPs

Different from our previous work related to the mild reduction synthesis of PEI-coated Fe_3O_4 NPs,[34, 35] in this study, mild reduction of Fe(III) salt in the presence PGA led to the formation of PGA-stabilized Fe_3O_4 NPs (Fe_3O_4-PGA NPs) that were used for MR imaging of tumors (Scheme 1). The formed Fe_3O_4-PGA NPs were characterized *via* different techniques. XRD was used to characterize the crystal structure of the particles (Figure 1). The lattice spacings at 2θ of 30.1, 35.5, 43.0, 53.4, 57.0, and 62.6° are consistent with the [220], [311], [400], [422], [511], and [440] planes of the magnetite, confirming the formation of the Fe_3O_4 NPs. Some new peaks emerging at the lattice spacings of 22.96, 32.72, 40.54, 46.92, and 58.34° may be due to the presence of PGA modified onto the Fe_3O_4 NP surfaces.[37] Due to the quite large percentage of PGA in the hybrid Fe_3O_4-PGA NPs (see below the TGA data), these new peaks associated to PGA can be clearly seen. In contrast, naked Fe_3O_4 NPs prepared under the same experimental conditions just display the typical planes of the magnetite.

The size and morphology of the Fe_3O_4-PGA NPs were characterized by TEM (Figure 2). Clearly, the formed Fe_3O_4-PGA NPs display a spherical or semi-spherical shape with quite a uniform size distribution, in agreement with the literature.[34,] The mean particle size was estimated to be 5.3 ± 2.6 nm. It seems that PGA is able to stabilize the formation of the Fe_3O_4 NPs, in agreement with our previous work relating to the use of citric acid to stabilize Fe_3O_4 NPs.[38, 39] The hydrodynamic size of the formed particles was measured *via* dynamic light scattering (DLS). We show that the Fe_3O_4-PGA NPs have a hydrodynamic size of 217.5 nm (Figure S1, Electronic Supplementary Information, ESI), which is much larger than that measured by TEM. This could be ascribed to the fact that DLS measures the size of large aggregates of particles in aqueous solution that may consist of many single Fe_3O_4 NPs, while TEM just measures single Fe_3O_4 core NPs, in agreement with our previous reports.[36, 40]

FTIR spectroscopy was used to qualitatively confirm the PGA coating onto the surface of the Fe_3O_4 NPs (Figure 3). The strong absorption band at 590 cm^{-1} can be assigned to the Fe-O bond of Fe_3O_4.[33] The band at 1637 cm^{-1} corresponds to the C=O stretching vibration of the PGA carboxyl groups, which is much more prominent than that of the naked Fe_3O_4 NPs, indicating the successful coating of PGA onto the surface of the Fe_3O_4 NPs. The coating of PGA onto the Fe_3O_4 NPs was also quantitatively characterized by TGA (Figure S2, ESI). The amount of PGA coated onto the Fe_3O_4 NPs was calculated to be 38.9%. Finally, the coating of PGA onto the Fe_3O_4 NP surfaces rendered the particles with a negative surface potential (-38.6 mV), which makes them quite colloidally stable. The particles dispersed in water, NS, and cell culture medium do not precipitate after stored at room temperature for at least two weeks (Figure S3, ESI), which is amenable for their further biomedical applications.

T_2 relaxometry

To explore the potential to use the Fe_3O_4-PGA NPs for MR imaging applications, T_2 relaxometry of the particles dispersed in water was performed (Figure 4). With the increase of Fe concentration, the Fe_3O_4-PGA NPs are able to decrease the MR signal intensity in the T_2-weighted MR images (Figure 4a). By linear fitting of the T_2 relaxation rate ($1/T_2$) as a function of Fe concentration (Figure 4b), the r_2 relaxivity of the Fe_3O_4-PGA NPs was estimated to be 333.7 $mM^{-1}s^{-1}$, which is much higher than that of other Fe_3O_4 NPs reported in the literature.[8, 31, 32] The

higher r_2 relaxivity is likely due to the nature of the mild reduction synthetic method that can be used to generate particles with super-high magnetic dipole interactions.[34, 35] Therefore, the developed Fe_3O_4-PGA NPs may be used as a good T_2 negative contrast agent for sensitive MR imaging applications.

Hemolysis assay

Hemocompatibility has been considered to be one of the most important issues that needs to be addressed before *in vivo* biomedical applications. As shown in the photographs (Figure S4, ESI), there is no obvious hemolysis phenomenon when HRBCs were exposed to the aqueous solutions of the Fe_3O_4-PGA NPs with different Fe concentrations (50, 150, 250, 350, and 450 μgmL^{-1}, respectively), which is similar to the negative NS control. In contrast, the HRBCs exposed to water (positive control) exhibit an apparent hemolysis phenomena. Further quantitative analysis reveals that the hemolysis percentages of HRBCs exposed to the Fe_3O_4-PGA NPs in the studied concentration range (50-450 μgmL^{-1}) are all less than 5% (a threshold value),[34, 35] confirming their excellent hemocompatibility.

Cytotoxicity assay

The *in vitro* cytotoxicity of the Fe_3O_4-PGA NPs was next assessed by MTT cell viability assay (Figure 5). Clearly, the viability of HeLa cells is not impacted after treated with the Fe_3O_4-PGA NPs at different Fe concentrations when compared with the NS control. The gradually increased cell viability is likely attributed to the excellent biocompatibility of PGA, which may slightly promote the growth of cells. In contrast, cells treated with the naked Fe_3O_4 NPs display decreased viability with the Fe concentration when compared with the NS control. These results indicate that the developed Fe_3O_4-PGA NPs are non-cytotoxic at the Fe concentration up to 450 μgmL^{-1}.

The cytocompatibility of the Fe_3O_4-PGA NPs was further assessed by observation of the morphology of HeLa cells treated with the particles in the Fe concentration range of 50-450 μgmL^{-1} for 24 h (Figure S5, ESI). It is evident that HeLa cells treated with the Fe_3O_4-PGA NPs do not display any appreciable morphological changes when compared to the control cells treated with the NS (Figure S5a, ESI). Taken together with both the quantitative MTT assay data and the cell morphology observation results, we can safely conclude that the Fe_3O_4-PGA NPs are non-cytotoxic in the studied Fe concentration range

Macrophage cellular uptake

For tumor imaging applications, it is generally required that the developed NPs are able to have minimum macrophage cellular uptake, thereby having prolonged blood half life for the particles to be accumulated into the tumor site through passive enhanced permeability and retention (EPR) effect.[31, 41-43] We next explored the macrophage cellular uptake of the Fe_3O_4-PGA NPs by ICP-OES (Figure 6). Compared with the naked Fe_3O_4 NPs, the Fe_3O_4-PGA NPs show much less Fe uptake, especially at a high Fe concentration (100 μgmL^{-1}). The PGA coating renders the particles to have about 40.5% decreased Fe uptake when compared to the naked Fe_3O_4 NPs. It seems that the strategy of PGA coating is powerful to confer the particles with significantly reduced macrophage cellular uptake, which is beneficial for the particles to escape from the RES and to accumulate in the tumor site for MR imaging applications.

***In vivo* MR imaging of a xenografted tumor model**

We next investigated the feasibility to use the developed Fe_3O_4-PGA NPs for MR imaging of a xenografted tumor model (Figure 7a). Clearly, starting at 2 h postinjection, the particles are able to induce a significant MR contrast enhancement in the liver, spleen, and tumor area, suggesting that the particles are able to be cleared by the RES-associated organs. Simultaneously, likely due to the PGA coating, a portion of particles are also able to escape from the RES and accumulate to the tumor tissue, enabling effective MR imaging of tumors. Different from the liver MR images that still have an appreciable MR contrast enhancement at 4 and 6 h postinjection, the tumor region seems to have the highest negative MR contrast enhancement at 2 h postinjection, and the MR signal intensity gradually recovers. By plotting the MR signal to noise ratio (SNR) as a function of the time postinjection, we were able to clearly observe the trend of MR SNR changes in the liver (Figure 7b) and in the tumor region (Figure 7c). Our results suggest that the formed Fe_3O_4-PGA NPs are able to be accumulated to tumor region through the passive EPR effect, allowing for effective MR imaging of tumors. At 4 h postinjection, the tumor MR SNR starts to be recovered, which is probably due to the fact that the particles have undergone a further metabolization process and have a decreased accumulation in the tumor region.

***In vivo* biodistribution**

To further explore the biodistribution behavior of the Fe_3O_4-PGA NPs *in vivo*, ICP-OES was performed to analyze the Fe concentration in several major organs including the heart, liver, spleen, lung, kidney, and tumor (Figure S6, ESI). The Fe concentrations in all the organs and tumor tissue at different time points postinjection are higher than that of the control mice injected with NS. A majority of Fe uptake occurs in the RES-associated organs (the liver and spleen), and a small portion of Fe uptake in the other organs such as the heart, lung, kidney, and tumor can be found. Clearly, the liver and tumor display the peak Fe uptake at 2 h postinjection and gradually reduced Fe uptake with the time postinejction, corroborating the MR imaging results. The much higher spleen uptake of the particles than the liver could be due to the size and/or the suface characteristics of the particles, leading to different levels of particle uptake in the RES-associated organs, in agreement with our previous work.[8, 32, 34, 35]

Conclusion

In summary, we developed a convenient method to form the Fe_3O_4-PGA NPs for MR imaging of tumors. In the presence of PGA, mild reduction of Fe(III) salt enables the generation of the Fe_3O_4-PGA NPs. The formed Fe_3O_4-PGA NPs are water dispersible, colloidally stable, and hemocompatible and cytocompatible in the studied Fe concentration range. With the high r_2 relaxivity and reduced macrophage cellular uptake, the Fe_3O_4-PGA NPs can be used as a contrast agent for MR imaging of tumors thanks to the passive EPR effect. The developed Fe_3O_4-PGA NPs could be modified with targeting ligands or drugs through the PGA carboxyl-enabled conjugation chemistry, thereby providing a unique nanoplatform for theranostics of

different biological systems.

Acknowledgements

This research is financially supported by the National Natural Science Foundation of China (21273032, 81341050, and 81401458), the Program for Professor of Special Appointment (Eastern Scholar) at Shanghai Institutions of Higher Learning, and the Sino-German Center for Research Promotion (GZ899). C. P. thanks the financial support from the Shanghai Natural Science Foundation (14ZR1432400).

Notes and references

[a] *State Key Laboratory for Modification of Chemical Fibers and Polymer Materials, College of Materials Science and Engineering, Donghua University, Shanghai 201620, People's Republic of China*
[b] *Department of Radiology, Shanghai Tenth People's Hospital, School of Medicine, Tongji University, Shanghai 200072, People's Republic of China*
[c] *College of Chemistry, Chemical Engineering and Biotechnology, Donghua University, Shanghai 201620, People's Republic of China. E-mail: xshi@dhu.edu.cn*
[1] *ZhiboYu and Chen Peng contributed equally to this work.*

† **Electronic supplementary information (ESI) available**: additional experimental data.

1. X. Shi, S. H. Wang, S. D. Swanson, S. Ge, Z. Cao, M. E. Van Antwerp, K. J. Landmark and J. R. Baker, *Adv. Mater.*, 2008, **20**, 1671-1678.
2. Y. M. Huh, Y. W. Jun, H. T. Song, S. Kim, J. S. Choi, J. H. Lee, S. Yoon, K. S. Kim, J. S. Shin, J. S. Suh and J. Cheon, *J. Am. Chem. Soc.*, 2005, **127**, 12387-12391.
3. L. Guo, W. Ding and L.-M. Zheng, *J. Nanopart. Res.*, 2013, **15**, 1-9.
4. S. H. Wang, X. Shi, M. Van Antwerp, Z. Cao, S. D. Swanson, X. Bi and J. R. Baker, *Adv. Funct. Mater.*, 2007, **17**, 3043-3050.
5. S. Narayanan, B. N. Sathy, U. Mony, M. Koyakutty, S. V. Nair and D. Menon, *ACS Appl. Mater. Interfaces*, 2012, **4**, 251-260.
6. Y. W. Jun, J. T. Jang and J. Cheon, in *Bio-Applications of Nanoparticles*, ed. W. C. W. Chan, Springer-Verlag Berlin, Berlin, 2007, vol. 620, pp. 85-106.
7. X. J. Ji, R. P. Shao, A. M. Elliott, R. J. Stafford, E. Esparza-Coss, J. A. Bankson, G. Liang, Z. P. Luo, K. Park, J. T. Markert and C. Li, *J. Phys. Chem. C*, 2007, **111**, 6245-6251.
8. J. Li, L. Zheng, H. Cai, W. Sun, M. Shen, G. Zhang and X. Shi, *Biomaterials*, 2013, **34**, 8382-8392.
9. J. Li, X. Shi and M. Shen, *Part. Part. Syst. Charact*, 2014, **31**, 1223-1237.
10. C. C. Berry, S. Wells, S. Charles, G. Aitchison and A. S. Curtis, *Biomaterials*, 2004, **25**, 5405-5413.
11. A. Moore, E. Marecos, A. Bogdanov Jr and R. Weissleder, *Radiology*, 2000, **214**, 568-574.
12. E. Strable, J. W. Bulte, B. Moskowitz, K. Vivekanandan, M. Allen and T. Douglas, *Chem. Mater.*, 2001, **13**, 2201-2209.
13. X. Shi, T. P. Thomas, L. A. Myc, A. Kotlyar and J. R. Baker Jr, *Phys. Chem. Chem. Phys.*, 2007, **9**, 5712-5720.
14. M. Shen and X. Shi, *Nanoscale*, 2010, **2**, 1596-1610.
15. J. Zhi, Y. Wang, Y. Lu, J. Ma and G. Luo, *React. Funct. Polym.*, 2006, **66**, 1552-1558.
16. Y.-C. Chang and D.-H. Chen, *J. Colloid Interface Sci.*, 2005, **283**, 446-451.
17. J. Xie, C. Xu, N. Kohler, Y. Hou and S. Sun, *Adv. Mater.*, 2007, **19**, 3163-3166.
18. E. K. Larsen, T. Nielsen, T. Wittenborn, H. Birkedal, T. Vorup-Jensen, M. H. Jakobsen, L. Østergaard, M. R. Horsman, F. Besenbacher and K. A. Howard, *ACS Nano*, 2009, **3**, 1947-1951.
19. A. Masotti, A. Pitta, G. Ortaggi, M. Corti, C. Innocenti, A. Lascialfari, M. Marinone, P. Marzola, A. Daducci and A. Sbarbati, *Magn. Reson. Mater. Phy., Biol. Med*, 2009, **22**, 77-87.
20. L. Zhang, T. Wang, L. Li, C. Wang, Z. Su and J. Li, *Chem. Commun.*, 2012, **48**, 8706-8708.
21. R. Namgung, K. Singha, M. K. Yu, S. Jon, Y. S. Kim, Y. Ahn, I.-K. Park and W. J. Kim, *Biomaterials*, 2010, **31**, 4204-4213.
22. C. Li, *Adv. Drug Delivery Rev.*, 2002, **54**, 695-713.
23. F. Wang, M. Ishiguro, M. Mutsukado, K.-i. Fujita and T. Tanaka, *J. Agric. Food Chem.*, 2008, **56**, 4225-4228.
24. C. Li, D.-F. Yu, R. A. Newman, F. Cabral, L. C. Stephens, N. Hunter, L. Milas and S. Wallace, *Cancer Res.*, 1998, **58**, 2404-2409.
25. C. Li, R. A. Newman, Q.-P. Wu, S. Ke, W. Chen, T. Hutto, Z. Kan, M. D. Brannan, C. Charnsangavej and S. Wallace, *Cancer Chemother. Pharmacol.*, 2000, **46**, 416-422.
26. R. Duncan, *Nat. Rev. Cancer*, 2006, **6**, 688-701.
27. C. T. Tsao, C. H. Chang, Y. Y. Lin, M. F. Wu, J. L. Wang, T. H. Young, J. L. Han and K. H. Hsieh, *Carbohydr. Polym.*, 2011, **84**, 812-819.
28. M. Matsusaki and M. Akashi, *Biomacromolecules*, 2005, **6**, 3351-3356.
29. S. Wang, X. Cao, M. Shen, R. Guo, I. Bányai and X. Shi, *Colloids Surf., B*, 2012, **89**, 254-264.
30. S. G. Wang, J. Y. Zhu, M. W. Shen, M. F. Zhu and X. Y. Shi, *ACS Appl. Mater. Interfaces*, 2014, **6**, 2153-2161.
31. H. D. Cai, X. An, J. Cui, J. C. Li, S. H. Wen, K. G. Li, M. W. Shen, L. F. Zheng, G. X. Zhang and X. Y. Shi, *ACS Appl. Mater. Interfaces*, 2013, **5**, 1722-1731.
32. J. Li, Y. He, W. Sun, Y. Luo, H. Cai, Y. Pan, M. Shen, J. Xia and X. Shi, *Biomaterials*, 2014, **35**, 3666-3677.
33. J. Hong, D. Xu, J. Yu, P. Gong, H. Ma and S. Yao, *Nanotechnology*, 2007, **18**, 135608.
34. Y. Hu, J. Li, J. Yang, P. Wei, Y. Luo, L. Ding, W. Sun, G. Zhang, X. Shi and M. Shen, *Biomater. Sci.*, 2015, **3**, 721-732.
35. J. Li, Y. Hu, J. Yang, W. Sun, H. Cai, P. Wei, Y. Sun, G. Zhang, X. Shi and M. Shen, *J. Mater. Chem. B*, 2015, **3**, 5720-5730.
36. H. D. Cai, K. G. Li, M. W. Shen, S. H. Wen, Y. Luo, C. Peng, G. X. Zhang and X. Y. Shi, *J. Mater. Chem*, 2012, **22**, 15110-15120.
37. H. Y. Lee, Y. I. Jeong and K. C. Choi, *Int. J. Nanomed.*, 2011, **6**, 2879-2888.
38. Y. Luo, J. Yang, Y. Yan, J. Li, M. Shen, G. Zhang, S. Mignani and X. Shi, *Nanoscale*, 2015, **7**, 14538-14546.
39. J. Yang, Y. Luo, Y. Xu, J. Li, Z. Zhang, H. Wang, M. Shen, X. Shi and G. Zhang, *ACS Appl. Mater. Interfaces*, 2015, **7**, 5420-5428.
40. H. Liu, Y. H. Xu, S. H. Wen, J. Y. Zhu, L. F. Zheng, M. W. Shen, J. L. Zhao, G. X. Zhang and X. Y. Shi, *Polym. Chem.*, 2013, **4**, 1788-1795.
41. C. Peng, K. Li, X. Cao, T. Xiao, W. Hon, L. Zheng, R. Guo, M. Shen, G. Zhang and X. Shi, *Nanoscale*, 2012, **4**, 6768-6778.

42. S. Wen, Q. Zhao, X. An, J. Zhu, W. Hou, K. Li, Y. Huang, M. Shen, W. Zhu and X. Shi, *Adv. Healthcare Mater.*, 2014, **3**, 1568-1577.
43. B. Zhou, L. Zheng, C. Peng, D. Li, J. Li, S. Wen, M. Shen, G. Zhang and X. Shi, *ACS Appl. Mater. Interfaces*, 2014, **6**, 17190-17199.

Figure captions

Scheme 1. Schematic illustration of the formation of the Fe_3O_4-PGA NPs for MR imaging of tumors.

Figure 1. XRD pattern of the Fe_3O_4-PGA and the naked Fe_3O_4 NPs.

Figure 2. TEM micrograph and size distribution histogram of the Fe_3O_4-PGA NPs.

Figure 3. FTIR spectra of the naked Fe_3O_4 NPs, PGA, and the Fe_3O_4-PGA NPs.

Figure 4. Colored T_2-weighted MR images and linear fitting of $1/T_2$ of the Fe_3O_4-PGA NPs at different Fe concentartions.

Figure 5. MTT assay of HeLa cell viability after treated with NS (control) and the Fe_3O_4-PGA NPs at different Fe concentrations for 24 h.

Figure 6. Macrophage cellular uptake of the Fe_3O_4-PGA NPs with Fe concentrations of 0, 10, and 100 μgmL^{-1}, respectively.

Figure 7. *In vivo* T_2-weighted MR images (a) and MR signal to noise ratio (SNR) of liver (b) and tumor (c) before and at different time points postinjection of the Fe_3O_4-PGA NPs (0.1 mL in NS solution, [Fe] =1 $mgmL^{-1}$).

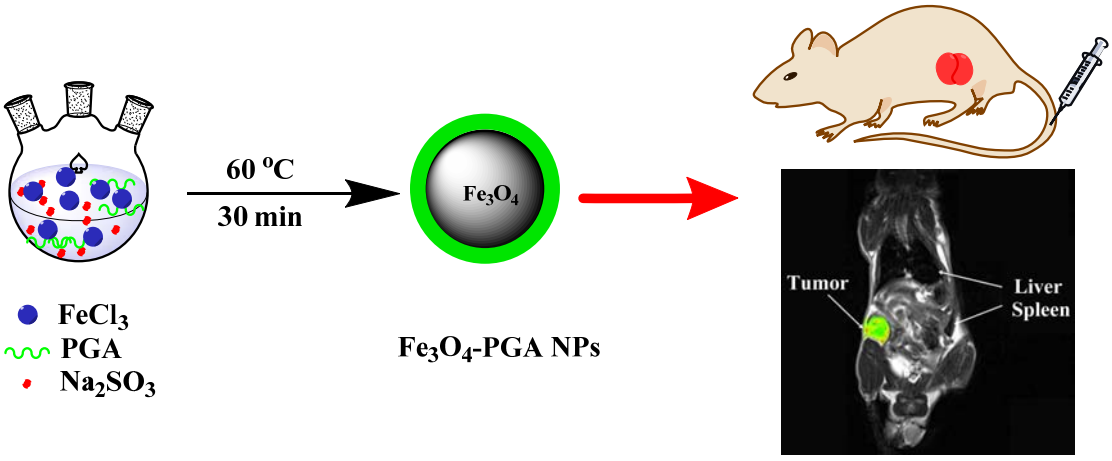

Scheme 1
Yu et al.

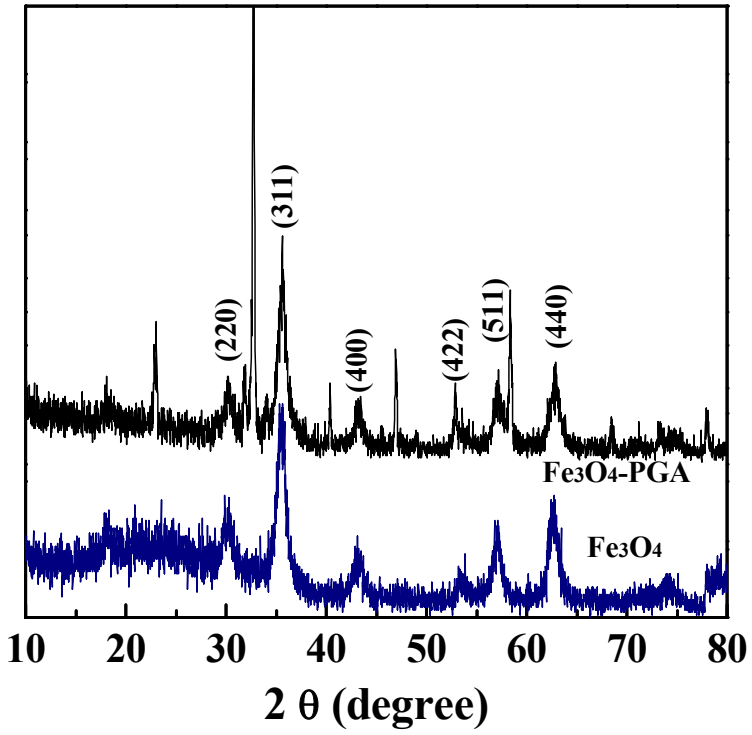

Figure 1
Yu et al.

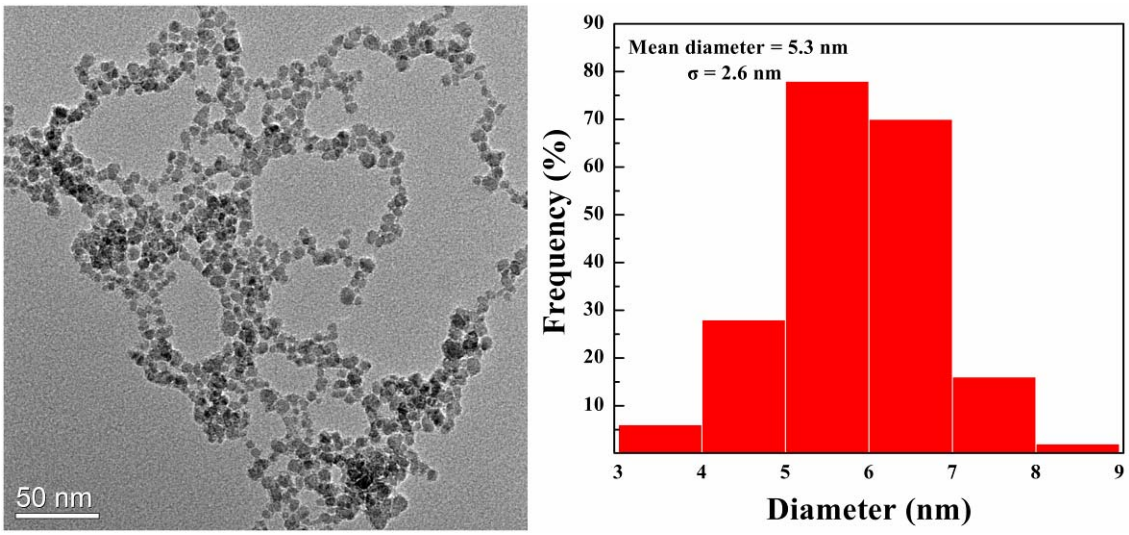

Figure 2
Yu et al.

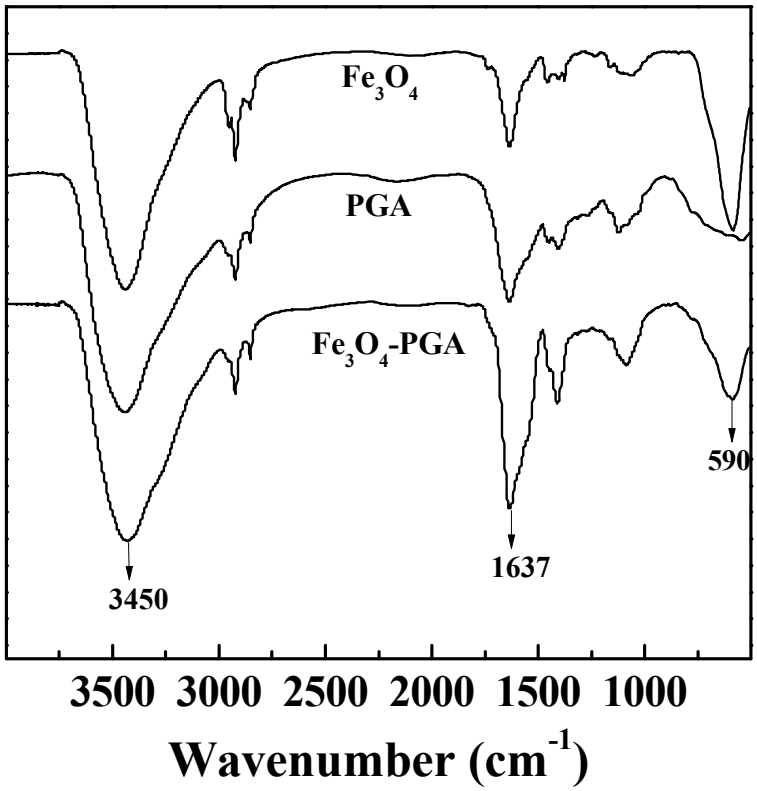

Figure 3
Yu et al.

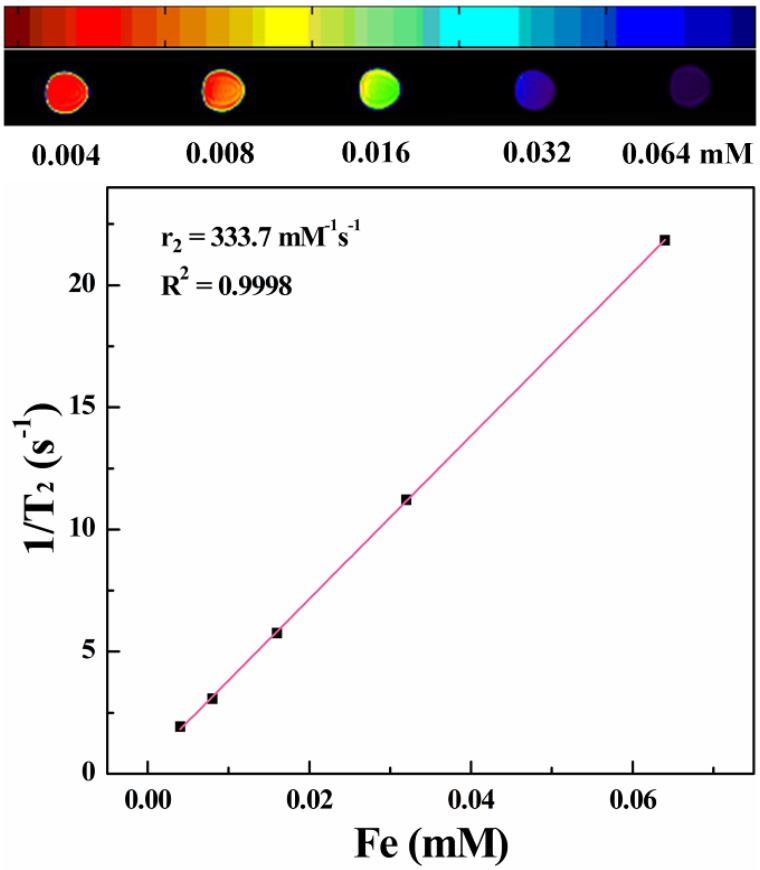

Figure 4
Yu et al.

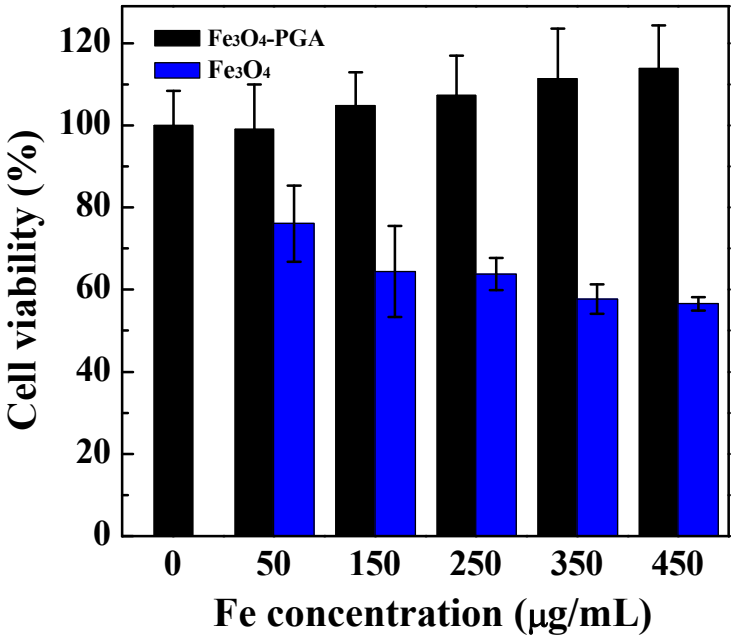

Figure 5
Yu et al.

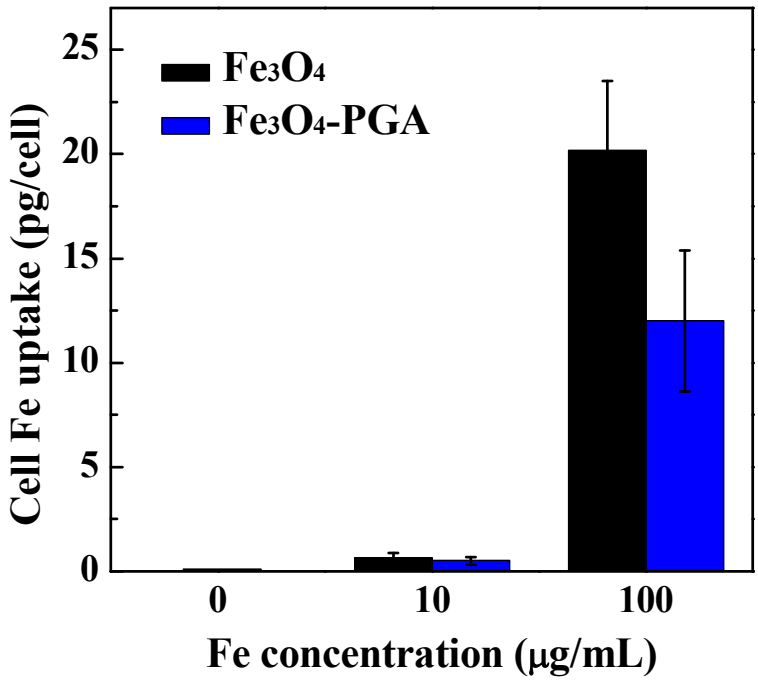

Figure 6
Yu et al.

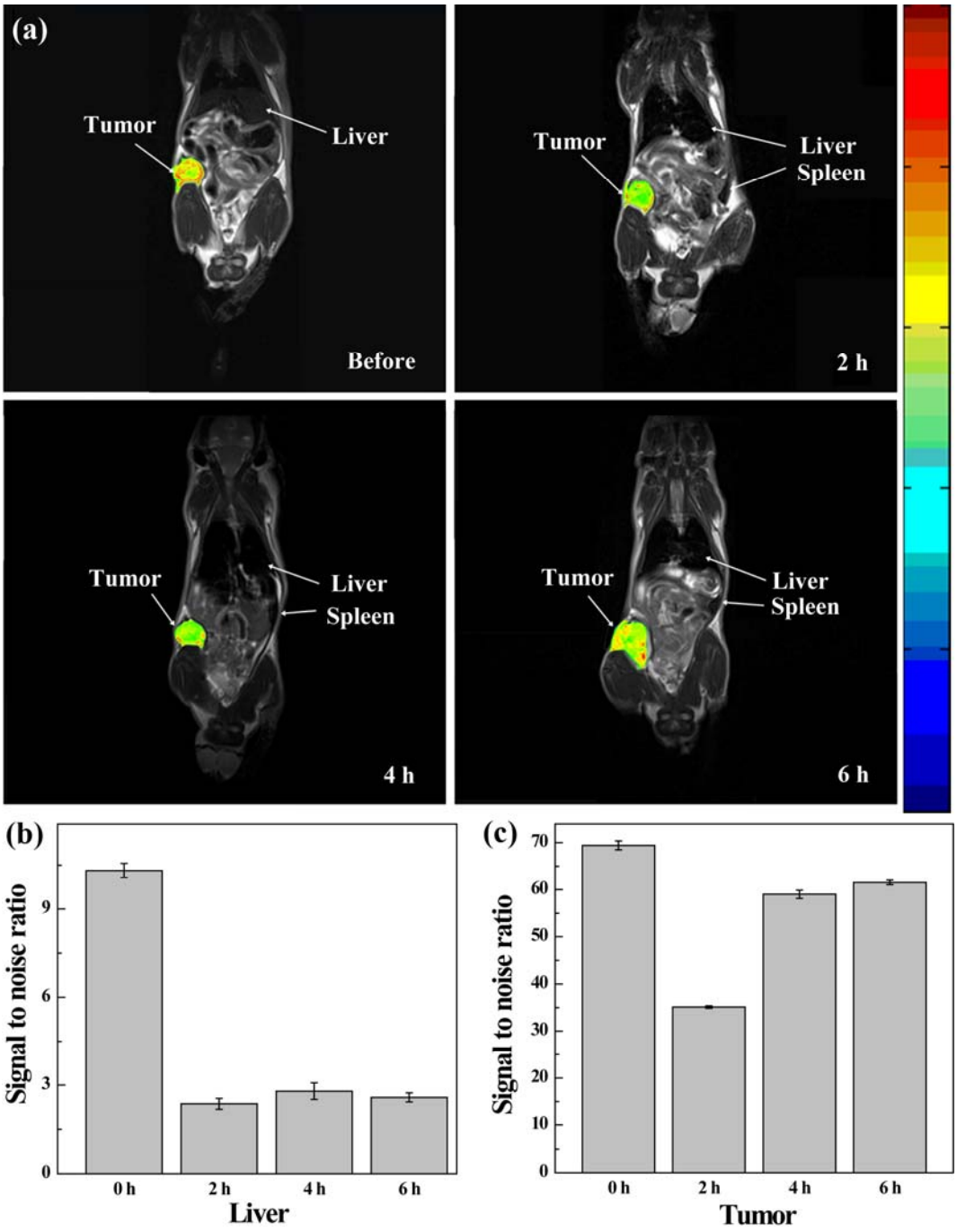

Figure 7
Yu et al.